IPTC-16600-MS

Influence of Micro-Computed Tomography Image Resolution on the Predictions of Petrophysical Properties

Nayef Alyafei, Imperial College (IC), Oussama Gharbi, IC, Ali Qaseminejad Raeini, IC, Jianhui Yang, IC, Stefan Iglauer, Curtin University, and Martin J. Blunt, IC

This paper was prepared for presentation at the International Petroleum Technology Conference held in Beijing, China, 26–28 March 2013.

Abstract

Micro-CT scanning is a non-destructive technique that can provide three-dimensional images of rock pore space at a resolution of a few microns. . However, these greyscale images cannot be directly input into simulators to predict flow properties; they require image processing to segment the solid and void space in the rock. Dynamic and static single phase properties can then be computed using the images directly or on extracted equivalent network models. In this paper, we study the effect of imaging resolution (five different voxel sizes ranging from 6-20 μm) of Clashach and Doddington sandstone on predicted single phase properties (porosity and absolute permeability) and network properties. Experimental data is used to validate the predictions. The results suggest that the computed porosity was largely independent of resolution and in good agreement with the measured value, while image resolutions of a few microns are sufficient to determine the permeability of a high-permeability rock such as Doddington but may not be sufficient for lower permeability samples. The topologically representative networks are sensitive to resolution, adding additional smaller pores and throats as the resolution is increased. This latter reason was confirmed by a network extraction analysis that indicated the average throat radius was 6 μm, similar to the highest resolution used and insufficient to image all important features of the pore space properly.

Introduction

Advances in three-dimensional digital imaging have allowed direct visualization of the pore space of many rocks (Dunsmuir et al., 1991; Coles et al., 1994; Lindquist and Venkatarangan, 1999; Wildenschild et al., 2002; Coenen et al., 2004; Wildenschild et al., 2005).These digital images can be obtained with micro-x-ray computerized tomography (micro-CT) without destroying the interior structure of the rock (Wildenschild et al., 2005). Pore-scale simulators require an accurate quantitative description of the microstructure (Arns et al., 2002); the level of detail that is observed, however, depends on the machine resolution (Wildenschild et al., 2005). This paper will study how image resolution affects predicted flow properties.

There are two approaches for computing flow and transport based on a three-dimensional representation of the pore space. The first is to compute the flow field directly on images using finite difference or particle-based methods (see, for instance (Boek and Venturoli, 2010; Mostaghimi et al., 2010). The second approach to extract a topologically representative network of pores and throats, and to compute flow through the network (Silin et al., 2003; Al-Kharusi and Blunt, 2007; Dong and Blunt, 2009). While this second approach simplifies the geometry of the pore space, it enables displacement in each network element to be computed semi-analytically. It is very effcient for the determination of multiphase flow properties where capillary forces dominate [(Blunt and King, 1992; Øren and Bakke, 2003; Valvatne and Blunt, 2004; Piri and Blunt, 2005a,b)]. In this paper we will also study the impact of image resolution on the properties of the extracted networks.

Experimental Methodology

We obtained micro-CT scans of dry cylindrical cores of Clashach and Doddington sandstone (diameter 4.95 mm, length 10 mm) with a v/tome/x Phoenix instrument at five different voxel sizes that we will assume is the resolution (5.789 μm, 8.946 μm, 11.972 μm, 14.998 μm and 19.997 μm) for Clashach and (5.999 μm, 8.996 μm, 11.972 μm, 14.998 μm and 19.997 μm) for Doddington. For convenience we will label these resolutions as 6 μm, 9 μm, 12 μm, 15 μm, and 20 μm for both samples.
Clashach sandstone is from northeast Scotland, UK. This sandstone is of Permian age and aeolian in origin, consisting of about 90% quartz and K-feldspar (Ngwenya et al., 1995). Doddington sandstone is from the Doddington quarry at Wooler, UK. This

sandstone is from the Carboniferous period and non-fossiliferous, consisting of approximately 95.2 % silica by weight with some white micas and feldspars (Santarelli and Brown, 1989). In an independent experiment, porosity (ϕ) was measured on a larger standard cylindrical core (diameter 38.1 mm, length 75 mm) via Helium pycnometry (Clashach porosity= 0.122 and Doddington= 0.207). Brine permeability (k) was measured on the large core (Clashach k= 80 mD [$7.9\text{x}10^{-14}$ m^2] and Doddington k= 2178 md [$2.1\text{x}10^{-12}$ m^2]) in a standard Hassler cell (Iglauer et al., 2010; Pentland et al., 2010). To guarantee consistency, the small and the large cores were drilled out of the same block.

Results and Disscusion

Micro-CT Images

The five different resolutions of Clashach were cropped to 300 × 300 × 300, 194 × 194 × 194, 145 × 145 × 145, 116 × 116 × 116, and 87 × 87 × 87 voxels to represent, approximately, the same volume of rock in each case. Similarly, for Doddington images of 300 × 300 × 300, 200 × 200 × 200, 150 × 150 × 150, 120 × 120 × 120, and 90 × 90 × 90 voxels were used. The rock volume was 5.8 mm^3 for Clashach and 5.2 mm^3 for Doddington with a difference of no more than 0.5% for the different resolutions. All the images represent the same piece of rock and were cropped in order to get the same volume. **Figure 1** shows the 3D images of the maximum and minimum resolution scans of both Clashach and Doddington. The images were filterd using a 3×3 median filter and then segmented according to Otsu's algorahim (Otsu, 1975). After that, a topological equavilent network of pores and throats were extracted.

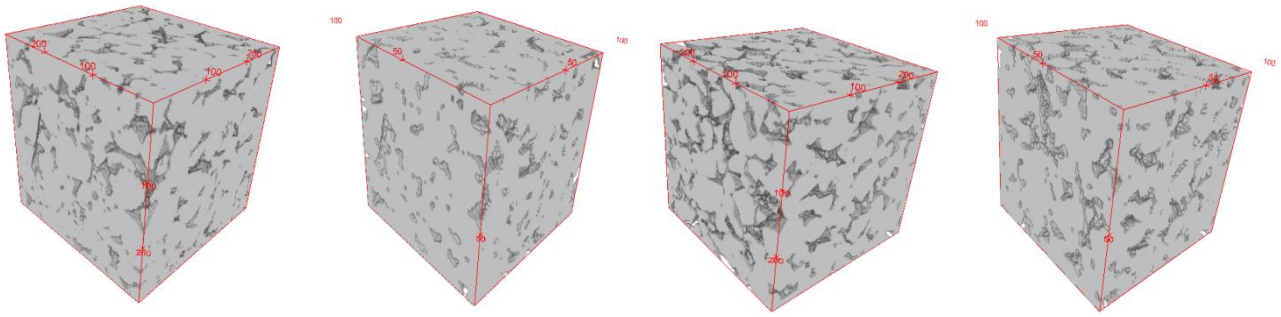

(a) (b) (c) (d)

FIG. 1: Three-dimensional micro-CT images used in this study on a) Clashach with 6 µm voxel edge length, b) Clashach with 20 µm voxel edge length, c) Doddington with 6 µm voxel length, and d) Doddington with 20 µm voxel edge length.

Petrophysical properties

Pore Network Properties

We use a maximal ball algorithm to extract topologically representative networks from the images. The method uses an algorithm where the largest spheres that fit in the pore space are pores, while chains of smaller spheres connecting them represent throats. Details of the method are provided elsewhere (Dong and Blunt, 2009). **Figure 2** shows the 3D images of the extracted networks of the maximum and minimum resolution scans of both Clashach and Doddington. We compare both sandstones in terms of numbers of pores, throats, coordination numbers (average number of throats connected to each pore), aspect ratios, pore radii, and throat radii. **Figures 3 and 4** show the distribution of the pore radii and throat radii respectively. As might be expected, the distributions for different image resolution are similar when the pore and throat radii are greater than the resolution itself; however, as finer details of the pore space are revealed, more small pores and throats are found. The pore and throat size distributions peak near the image resolution and more pores and throats are found for the finer resolutions. The distributions for the two sandstones are similar with slightly larger pores and throats for Doddington. Figure 5a shows increasing average pore radii for both sandstones as we decrease the resolution. There is only a slight difference between both sandstones: Doddington has slightly larger pores and throats consistent with a higher permeability; however, the difference in size is too small to explain the significant difference in the permeability. We show later that this is controlled by the connectivity of the pore space. **Figure 5b** shows that the average throat radii decrease with image resolution, since the extraction algorithms uncovers smaller features of the pore space; the average throat radius is close to the resolution of the scans, indicating that the behaviour is dominated by the smallest resolvable features.

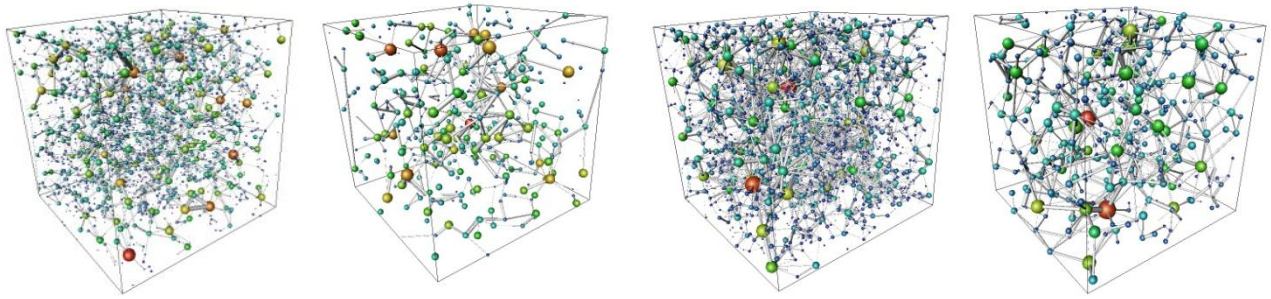

(a) (b) (c) (d)

FIG. 2: Three-dimensional pore and throat images (generated from the network extraction code (Dong and Blunt, 2009)on a) Clashach with 6 µm voxel edge length, b) Clashach with 20 µm voxel edge length, c) Doddington with 6µm voxel length, and d)Doddington with 20 µm voxel edge length.

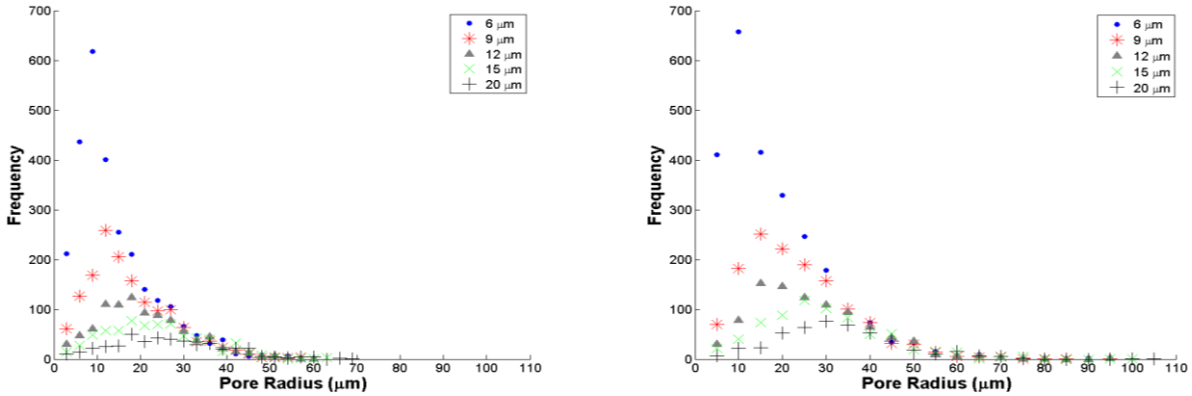

(a) (b)

Fig. 3: Pore radius distribution from the extracted network for (a) Clashach and (b) Doddington. The image resolution is shown in the legend.

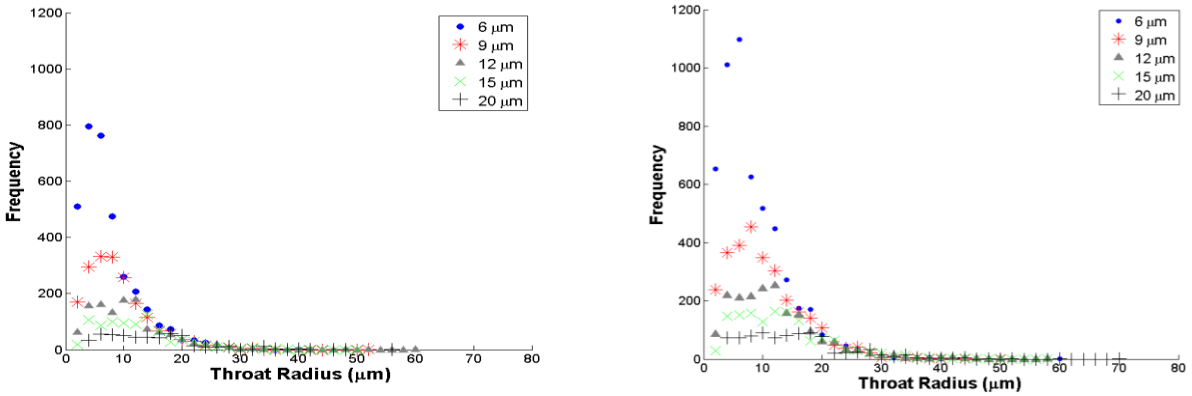

(a) (b)

Fig. 4: Throat radius distribution from the extracted network for (a) Clashach and (b) Doddington. The image resolution is shown in the legend.

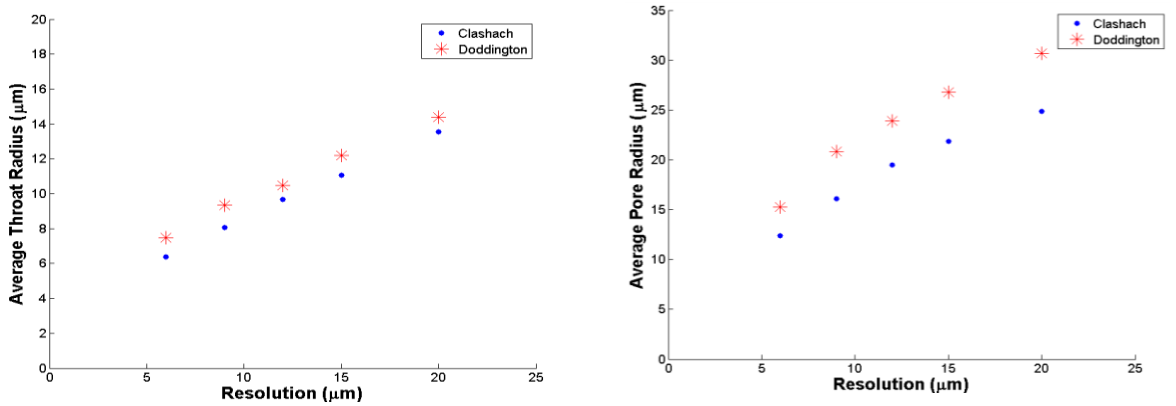

(a) (b)

Fig. 5: (a) Average pore radius (b) average throat radius, as a function of image resolution for Clashach and Doddington.

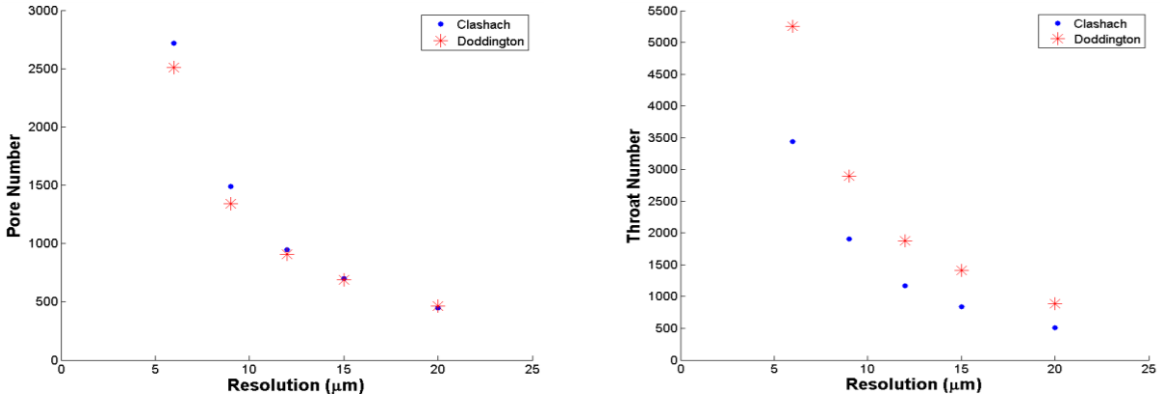

(a) (b)

Fig. 6: (a) Number of pores, and (b) number of throats, as a function of image resolution for Clashach and Doddington.

Figure 6a and 6b show the number of pores and throats as a function of resolution of both sandstones respectively.The number of pores and throats increases with resolution: the network extraction clearly does not identify a unique structure, but, as the image is refined, finds more network elements of smaller size (see later for further discussion).

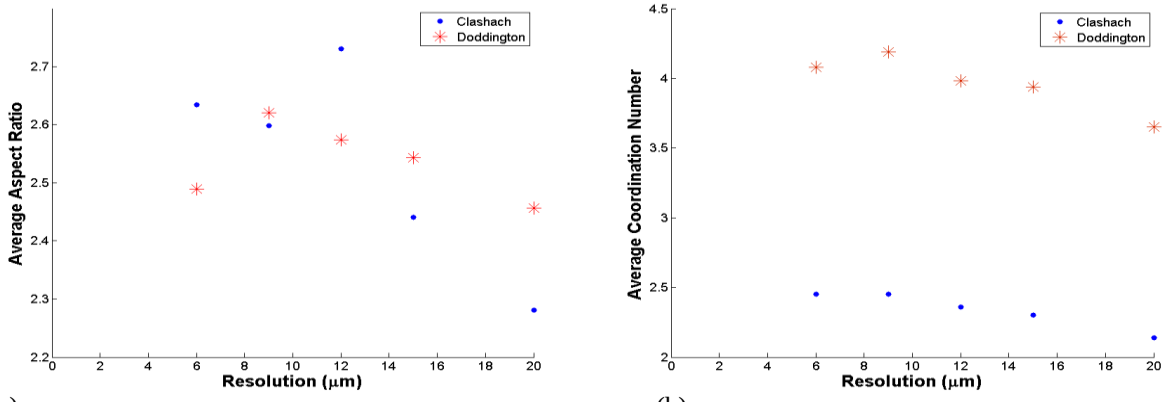

(a) (b)

Fig. 7: (a) Average aspect ratio: the average ratio of pore radius to the mean radius of connected throats, and (b) average coordination number, as a function of image resolution for Clashach and Doddington.

Figure 7a shows the aspect ratio which is the ratio of the pore radius to throat radius. The aspect ratio was calculated using the following equation:

$$\alpha = \sum_{j=1}^{n_p} \frac{n_c r_{pj}}{\sum_{i=1}^{n_{cj}} r_{tij}} \quad (1)$$

where r_p is the pore radius, n_{cj} is the coordination number for pore j (the number of throats connected to that pore), and r_t the throat radius; j labels the pores and n_p is the total number of pores, while ij labels the throats connected to pore j. For both sandstones the values are similar around - 2.5 - with little change with resolution. The reason for this is that with increased resolution, smaller pores and throats are extracted, but the ratio of their sizes remains largely unchanged. Aspect ratio is important as it controls the trapping of the non-wetting phase by snap-off (Lake, 1989).

Figure 7b shows the average coordination number as a function of image resolution. For both sandstones we observe an almost constant trend – again as smaller pores and throats are extracted, we see the same ratio of the number of throats to pores. However, Doddington has a higher coordination number compared to Clashach, implying a more connected pore space, which is consistent with Doddington's higher permeability. For these samples the connectivity is a greater control on the permeability than pore size.

Surface Area, Porosity, and Permeability

The porosity and surface area of the images are shown in **Table 1**. Porosity is relatively insensitive to resolution, with a small increase as resolution is improved and some smaller features of the pore space are revealed. The computed values, based on the thresholded images, are close to the experimentally measured values. The specific surface area is the area of interface between pore and grain - computed on the images per unit volume. As expected, the surface area increases with improved resolution as finer features of the pore space are captured. The specific surface area is the inverse of a typical length scale - a typical grain size – of around 100 μm - but also represents the roughness of the grains. With a finer resolution, more roughness is uncovered. Doddington has a larger specific surface area, consistent with a better connected pore space.

Table 1: Surface area and porosity of Clashach and Doddington images

Resolution (μm)	6	9	12	15	20	Experimental
Sample name	Clashach					
Specific surface area (m^{-1})	16100	13100	11700	10600	9280	
Porosity (%)	12.2	11.5	11.6	11.6	11.7	12.2
Sample name	Doddington					
Specific surface area (m^{-1})	20900	17800	15400	14200	12500	
Porosity (%)	20.8	20.3	19.6	19.5	19.4	20.7

We then used three different simulators to calculate the single phase permeability. First we computed the permeability of the extracted networks: the computation essentially treats the porous medium as a random resistor network with semi-analytically computed permeabilities for each element (Valvatne and Blunt, 2004). The other simulations computed flow at low Reynold's number directly on the images using either a finite difference Stokes-flow simulator (OpenFOAM, 2010) or a lattice-Boltzmann code (Boek and Venturoli, 2010). **Figures 8, 9, and 10** show the predicted permeability using the extracted networks and direct images as a function of resolution for Clashach and Doddington. All the simulation runs were performed for flow in the three coordinate directions (x, y, z) in order to evaluate the anisotropy: a constant pressure drop was applied across the main flow direction with no flow across the other faces. As the resolution improves, the predicted permeability tends to increases, as more flow channels are observed. As expected, the two methods to compute the permeability directly on the image agree well in most cases, although the results are not identical, since the algorithms used to compute the flow are very different. In particular, for small flow channels, the methods are sensitive to resolution; for instance in lattice-Boltzmann simulation, we need at least four nodes between grains to obtain acceptable accuracy, while we know from our network analysis that many of the flow channels are only one or two voxels across (Sukop and Thorne, 2006). The networks tend to give lower predicted permeabilities, indicating that some connectivity of the pore space is lost; as more small pores and throats are extracted, the computed permeability increases. At the highest resolution studied there is reasonable agreement between the predicted values and little evidence of signiffcant anisotropy. For Doddington, with a well-connected pore space there is good agreement between predicted and measured permeability, with an indication that for infinite resolution the results would converge on a result slightly higher than the core-measured value. For Clashach, however, it is clear that the predicted values are all signiffcantly higher than the measured permeability. Here, the pore space is less well connected and it is likely that the rock is heterogenous at the mm scale, meaning that the average permeability of the core of volume 86,000 mm^3 (length 75 mm and diameter 38.1 mm) is likely to be different from that computed on a sample volume 5.8 mm^3 even though the predicted and measured porosities are in good agreement (Lake, 1989).

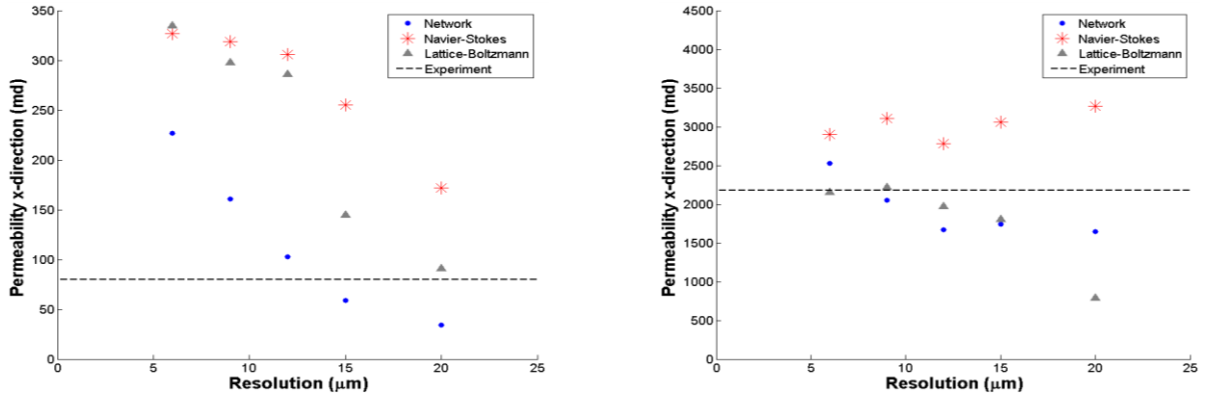

(a) (b)

Fig. 8: Predicted permeability in the x-direction in millidarcy for each image resolution of (a) Clashach and (b) Doddington, compared to the experimental value.

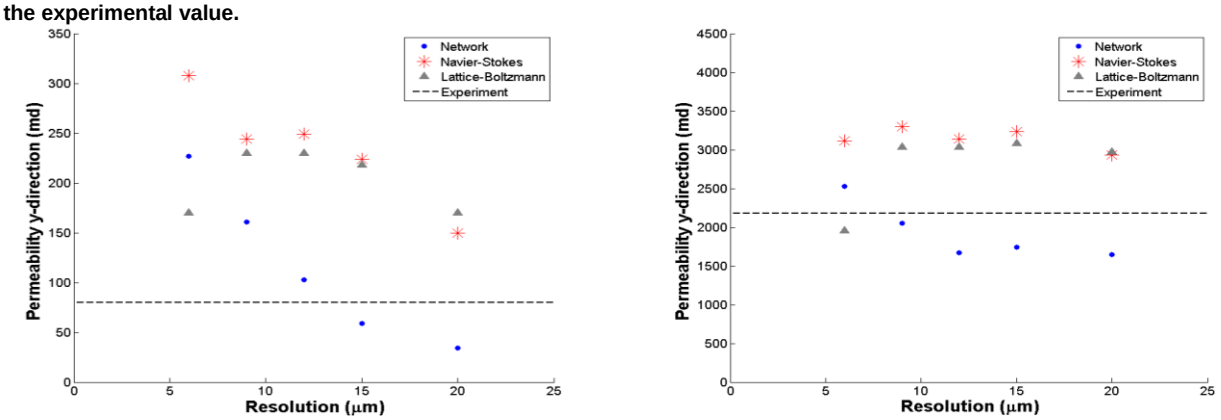

(a) (b)

Fig. 9: Predicted permeability in the y-direction in millidarcy for each image resolution of (a) Clashach and (b) Doddington, compared to the experimental value.

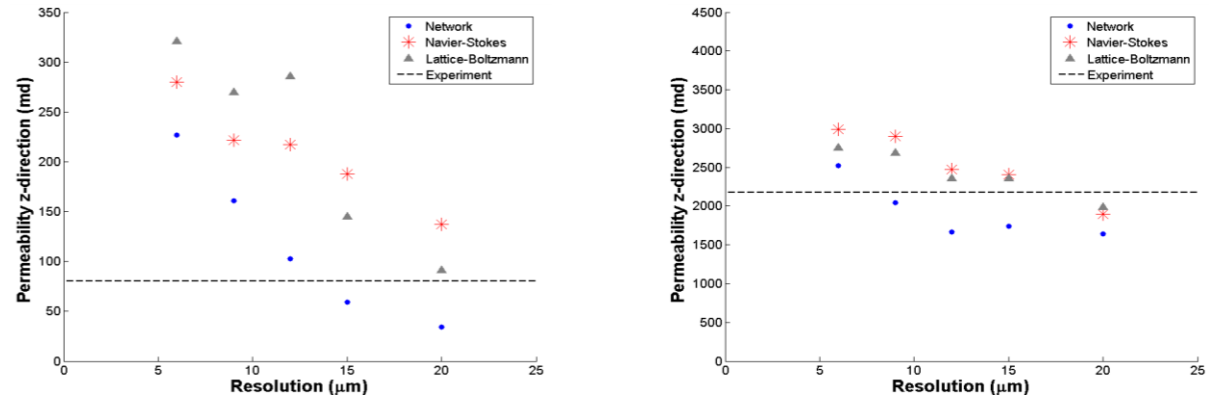

(a) (b)

Fig. 10: Predicted permeability in the y-direction in millidarcy for each image resolution of (a) Clashach and (b) Doddington, compared to the experimental value.

Conclusions

We have determined the impact of image resolution on extracted networks and computed flow properties for two sandstone samples. For the images studied, current extraction techniques do not appear to produce a unique network, with more pores and throats revealed as the image resolution is refined; the average throat radius is close to the image resolution, indicating that a resolution of 6 μm isinsuficient to converge on a network for these sandstones. However, the permeability computed on these networks, and directly on the images themselves, do show some degree of convergence. For better connected, high-permeability sandstone, the predicted permeability was in good agreement with that measured on a larger core sample of the same rock. For the lower-permeability sandstone, with a more poorly connected pore space, the predicted permeability was much higher than the core measurement, indicating mm-scale heterogeneity. The overall conclusion of this study is that micro-

CT images with a resolution of 5-10 µm may be suffcient to determine flow properties of homogenous high-permeability sandstones, but higher resolution may be required or larger images for lower permeability and more heterogeneous samples. The extracted networks are not unique, but give predictions of permeability that are within 50% of direct computations on the image for the highest resolution studied. It is the topic of future work to determine how image resolution affects the predictionsof multiphase flow properties, such as relative permeability.

Acknowledgments

We would like to acknowledge funding from the Qatar Carbonates and Carbon Storage Research Centre, QCCSRC, which is supported jointly by Qatar Petroleum, Shell and the Qatar Science &Technology Park.

Referances

Al-Kharusi, A.S. and Blunt, M.J. 2006. Network Extraction from Sandstoneand Carbonate Pore Space Images. *Journal of Petroleum Science and Engineering* **56**: 219-231.

Arns, C. H., Knackstedt, M.A., Val Pinczewski, W., and Garboczi, E.J. 2002. Computation of Linear Elastic Properties from Microtomographic Images: Methodology and Agreement Between Theory and Experiment. *Geophysics* **67**. doi: 10.1190/1.1512785.

Blunt, M. and King, M.J. 1992. Simulation and Theory of Two-phase Flow in Porous Media. *Phys Rev A* **46**. doi: 10.1103/PhysRevA.46.7680.

Boek, E. S., and Venturoli, M. 2010. Lattice-Boltzmann Studies of Fluid Flow in Porous Media with Realistic Rock Geometries. *Computers & Mathematics with Applications* **59(7)**: 2305-2314.

Coenen, J., Tchouparova, E. and Jing, X. 2004. Measurement Parameters and Resolution Aspects of Micro X-ray Tomogrraphy for Advanced Core Analysis. Proceedings of International Symposium of Society of Core Analysts, Abu Dhabi, UAE.

Coles, M. E., P. Spanne, E. L. Muegge, and K. W. Jones. 1994. Computed Microtomography of Reservoir Core Samples. In Proceedings of the 1994 Annual SCA Meeting, pp. 12-14.

Dong, H. and Blunt, M.J. 2009. Pore-Network Extraction from Micro-Computerized-Tomography Images. *Phys. Rev. E* **80**. doi: 10.1103/PhysRevE.80.036307.

Dunsmuir, J. H., Ferguson, S. R., D'Amico, K. L., and Stokes, J. P. 1991. X-ray Microtomography: a New Tool for the Characterization of Porous Media. In SPE Annual Technical Conference and Exhibition.

Iglauer, S., Favretto, S., Spinelli, G., Schena, G., and Blunt, M.J. 2010. X-ray Tomography Measurements of Power-Law Cluster Size Distributions for the Nonwetting Phase in Sandstones. *Phys. Rev. E***82**. doi: 10.1103/PhysRevE.82.056315.

Lake, L. W.1989. *Enhanced Oil Recovery*. Old Tappan, NJ: Prentice Hall Inc.

Lindquist, W. B., and Venkatarangan, A. 1999. Investigating 3D Geometry of Porous Media from High Resolution Images. *Physics and Chemistry of the Earth, Part A: Solid Earth and Geodesy* **24(7)**: 593-599.

Ngwenya, B. T., Elphick, S. C., and Shimmield, G. B. 1995. Reservoir Sensitivity to Water Flooding: An Experimental Study of Seawater Injection in a North Sea Reservoir Analog. *AAPG bulletin* **79(2)**: 285-303.

OpenFOAM. 2010. The open source CFD toolbox.Retrieved 25 June 2010, from http://www.openfoam.com.

Øren, P. and Bakke, S. 2002. Process Based Reconstruction of Sandstones and Prediction of Transport Properties. *Transport in Porous Media* **46**, 311.

Otsu, N. 1975. A Threshold Selection Method from Gray-Level Histograms. *Automatica* **11(285-296)**: 23-27.

Pentland, C.H., Tanino, Y., Iglauer, S., and Blunt, M.J. 2010. Capillary Trapping in Water-Wet Sandstone: Coreflooding Experiments and Pore-Network Modelling. Paper SPE 133798 proceedings of the SPE Annual Technical Conference and Exhibtion, Florence, Italy, 19-22 September. doi:10.2118/133798-MS.

Mostaghimi, P., Bijeljic, B., and Blunt, M. J. 2010. Simulation of Flow and Dispersion on Pore-Space Images. Paper SPE 135261 proceedings of the SPE Annual Technical Conference and Exhibtion, Florence, Italy, 19-22 September. doi:10.2118/135261-MS.

Piri, M. and Blunt, M.J. 2005. Three-dimensional Mixed-Wet Random Pore-Scale Network Modeling of Two-and Three-Phase Flow in Porous Media. I. Model Description. *Phys Rev E***71**. doi 10.1103/PhysRevE.71.026301.

Piri, M. and Blunt, M.J. 2005. Three-Dimensional Mixed-Wet Random Pore-Scale Network Modeling of Two-and Three-Phase Flow in Porous Media. II. Results. *Phys. Rev. E***71**. doi: 10.1103/PhysRevE.71.026302.

Santarelli, F. J., and Brown, E. T. 1989. Failure of Three Sedimentary Rocks in Triaxial and Hollow Cylinder Compression Tests. I*nternational Journal of Rock Mechanics and Mining Sciences & Geomechanics Abstracts* (Vol. 26, No. 5, pp. 401-413).

Silin, D.B., Jin, G., and Patzek, T. W. 2003. Robust Determination of Pore Space Morphology in Sedimentry Rocks. Paper SPE 84296 proceedings of the SPE Annual Technical Conference and Exhibition, Denver, Colorado, USA, 5-8 October. doi:10.2118/84296-MS

Sukop, M. C. and Thorne, D. T. 2006. *Lattice Boltzmann Modeling: An Introduction for Geoscientists and Engineers*. Springer.

Valvatne, P. and Blunt, M.J. 2004. Predictive Pore-Scale Modeling of Two-Phase Flow in Mixed Wet Media. *Water Resour*. *Res* **40,** W07406. doi: 10.1029/2003 WR002627

Wildenschild, D., Hopmans, J. W., Rivers, M. L., and Kent, A. J. R. 2005. Quantitative Analysis of Flow Processes in a Sand Using Synchrotron-Based X-ray Microtomography. *Vadose Zone Journal* **4(1)**: 112-126.

Wildenschild, D., Vaz, C. M. P., Rivers, M. L., Rikard, D., and Christensen, B. S. B. 2002. Using X-ray Computed Tomography in Hydrology: Systems, Rsolutions, and Limitations. *Journal of Hydrology* **267(3)**: 285-297.